Icarus 308 (2018) 128–137

Contents lists available at ScienceDirect

Icarus

journal homepage: www.elsevier.com/locate/icarus

Earliest accumulation history of the north polar layered deposits, Mars from SHARAD

Stefano Nerozzi*, John W. Holt

Institute for Geophysics, Jackson School of Geosciences, The University of Texas at Austin, 10100 Burnet Road, R2200, Austin, TX 78758-4445, USA

ARTICLE INFO

Article history:
Received 1 February 2017
Revised 19 May 2017
Accepted 31 May 2017
Available online 7 June 2017

ABSTRACT

The approximately 2 km thick north polar layered deposits (NPLD) are often considered to contain the most complete and detailed stratigraphic records of recent climate of Mars. Exposures of the dense layering within troughs and scarps allowed detailed reconstructions of the latest accumulation history of these water ice deposits, but we lack knowledge of their initial emplacement. The Shallow Radar (SHARAD) onboard Mars Reconnaissance Orbiter (MRO) penetrates the NPLD to their base and detects their internal layering, overcoming the limitation of scarce and scattered visible outcrops of the lowermost sequences.

In this study, we map reflectors in SHARAD data that result from discrete stratigraphic horizons in order to delineate the three-dimensional stratigraphy of the lowermost ~500 m NPLD sequence and reconstruct their accumulation history. We confirm the large-scale lateral continuity and thickness uniformity of the deposits previously detected within the lowermost NPLD. However, stratigraphic complexity—in the form of pinch-outs and significant thickness variations—arises when we examine single radar units. We find evidence of an initially limited geographic stability of water ice within two deposits that are centered at the North Pole and present-day Gemina Lingula. A period of lateral ice sheet growth followed, interrupted only once by a retreat episode. Lower net accumulation is observed on pre-existing slopes, suggesting a reduction of water ice stability due to increased solar radiation incidence and/or transport by katabatic winds. Lateral transport of water ice by wind is also suggested by thickness undulations toward the top of the sequence, resembling cyclic steps.

Water ice accumulation models based on orbital forcing predict a sequence of deposition and retreat events that is generally compatible with our reconstructed accumulation history. Therefore, we interpret the stratigraphic complexity that we observe as regional and, possibly global, climate change induced by orbital forcing. We also find that at least two units are completely buried within the NPLD and do not outcrop, and that NPLD deposition in some places was contemporaneous with deposition of the stratigraphically underlying cavi unit in other places. Both of these findings show that radar reflector mapping is a necessary complement to any stratigraphic reconstruction based on visible exposures.

1. Introduction

The north polar layered deposits (NPLD) are the largest accumulation of water ice in the northern hemisphere of Mars, and the second largest on the planet. The NPLD make up the upper part of Planum Boreum and lie over the Vastitas Borealis interior unit (H_{BV_i}) (Tanaka et al., 2008; Tanaka and Fortezzo, 2012) and the basal unit (BU), which is divided into the Rupēs unit and Cavi unit (Brothers et al., 2015; Byrne and Murray, 2002; Edgett et al., 2003; Fishbaugh and Head, 2005; Tanaka et al., 2008; Tanaka and Fortezzo, 2012) (Fig. 1). They consist of a dome-shaped deposit of water ice with up to 10% dust (Grima et al., 2009). Since their discovery (Soderblom et al., 1973), they are thought to hold a valuable record of recent climate change within their stratigraphy (Cutts, 1973), yet little is known about their initial accumulation history and significant uncertainties remain on their estimated age.

To first order, layering has been found to be laterally continuous and characterized by relatively uniform thicknesses throughout the NPLD by visual correlation of layer groups and single "marker beds" (Malin and Edgett, 2001), layer sequences (Fishbaugh and Hvidberg, 2006), spectrally detrended albedo matching (Milkovich and Head, 2005), layer topographic protrusion (Becerra et al., 2016) and radar mapping (Holt et al., 2010; Phillips et al., 2008; Putzig et al., 2009). Attempts have been made to constrain NPLD age by means of crater counting (Tanaka et al., 2008) and correlation of the apparently periodic layering with accumulation models based

* Corresponding author.
E-mail addresses: stefano.nerozzi@utexas.edu (S. Nerozzi), holt@utexas.edu (J. W. Holt).

http://dx.doi.org/10.1016/j.icarus.2017.05.027
0019-1035/

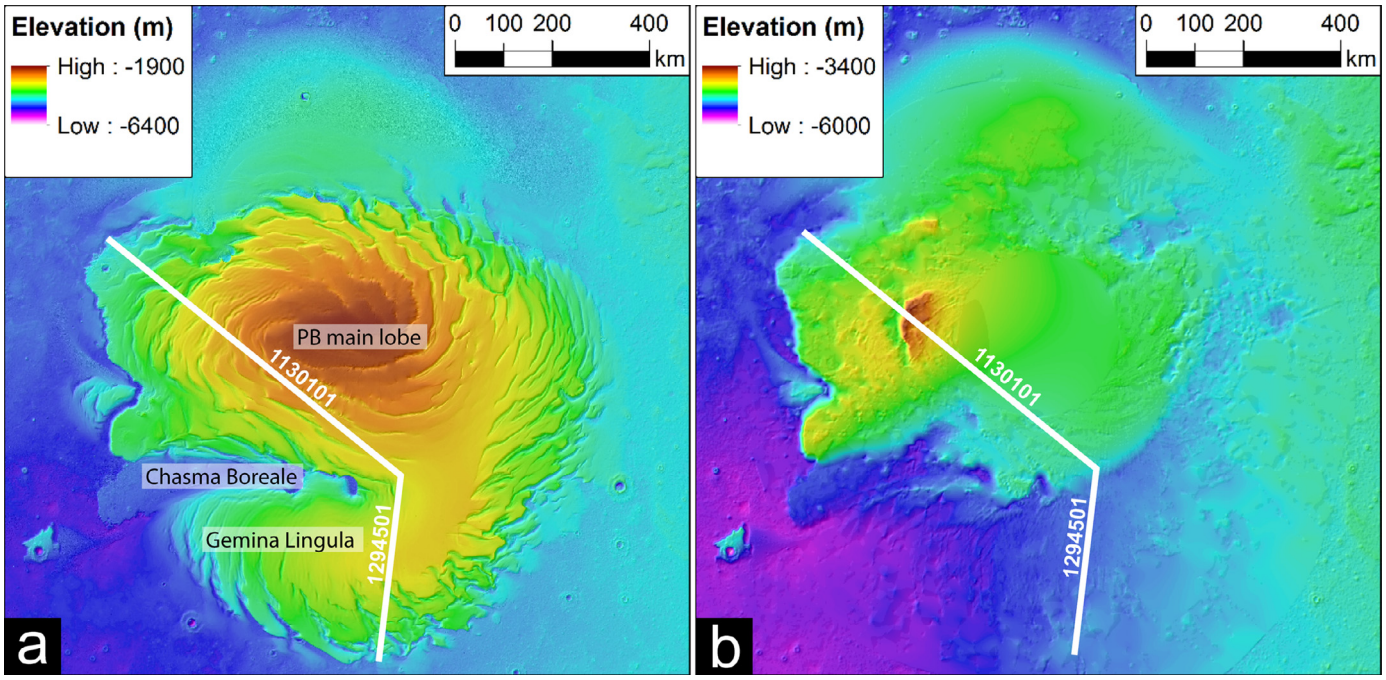

Fig. 1. Present and past Planum Boreum (PB) topography. (a) Mars Orbital Laser Altimeter (MOLA) surface elevation map of PB and surrounding plains. (b) Map of surface elevation prior to NPLD deposition, constructed by merging SHARAD mapping of BU top surface (modified from Brothers et al., 2015) with present surface adjacent to PB. White lines and numbers indicate the ground tracks of SHARAD profiles shown in Fig. 2.

on orbital forcing assumptions (Fishbaugh and Hvidberg, 2006; Hvidberg et al., 2012; Phillips et al., 2008; Putzig et al., 2009). Crater counting results are statistically weak and only constrain NPLD age to the Late Amazonian (Tanaka et al., 2008), and continuous resurfacing processes are capable of altering this record over timescales of 10^2–10^3 yr (Banks et al., 2010; Galla et al., 2008; Landis et al., 2016), therefore potentially biasing deposit age estimates to younger ages.

The correlation of fine scale stratigraphy exposed in troughs based on very high-resolution imagery allowed the construction of detailed accumulation models based on different orbital forcing parameters, in turn constraining the modeled age of the NPLD with higher precision (Hvidberg et al., 2012). However, the intrinsic stratigraphic complexity of the NPLD, mainly due to the presence of non-periodic brightness signals (Milkovich and Head, 2005), depositional and erosional hiatuses (Holt et al., 2010; Milkovich and Head, 2005; Phillips et al., 2008; Putzig et al., 2009; Tanaka et al., 2008) and presence of modern dust mantles (Fishbaugh et al., 2010), leads to non-unique solutions (e.g. Putzig et al., 2009) and may undermine the reliability of such accumulation models (Christian et al., 2013; Fishbaugh et al., 2010). In addition, because no detailed stratigraphic models of the lowermost NPLD are available, the accumulation models do not take into account the presence of possible hiatuses in the lowermost ~500 m of ice deposits. Thus, the first depositional events of the NPLD and their timing are still poorly constrained and only inferred from models extrapolating back in time from the overlying stratigraphic record.

The layering visible in optical images results from a combination of factors including different fractions of ice and entrained dust (Cutts, 1973; Cutts and Lewis, 1982; Thomas et al., 1992) in addition to surface morphology, which controls the local amount of surface dust and frost retention, both of which affect albedo (Fishbaugh et al., 2010). The distinction and correlation of layers across the NPLD at small scales within optical imagery is challenging to impossible in the lowermost sequences where outcrops are scarce.

Radar reflectors, instead, can be easily followed for hundreds of km (Phillips et al., 2008; Seu et al., 2007) and are inferred to originate from dielectric contrasts due to changing ratios of dust and water ice (Nunes and Phillips, 2006). Lalich and Holt (2016) showed that reflector properties in the NPLD are consistent with ~2–10 m thick, laterally extensive layers prominent at outcrops known as "marker beds" (Fishbaugh et al., 2010; Malin and Edgett, 2001).

SHARAD radargrams show a repeating stratigraphic pattern in the NPLD, generally consisting of four packets with many radar reflectors separated by three inter-packet regions with few or no reflections (Phillips et al., 2008). Putzig et al. (2009) further divide the lowermost packet into two different units: a 200–300 m packet ("Unit C") of quasi-parallel reflectors which overlies both the VBi unit and the BU, and an overlying wedge ("Unit D") of quasi-parallel reflectors up to 300 m thick confined in the Gemina Lingula region; both units are bound on top by an angular unconformity with "Unit E" .

The NPLD can also be subdivided into different units using an adapted sequence stratigraphy approach. Holt et al. (2010) mapped three main sequences bound by two angular unconformities. The lowermost unconformity delineates the proto-Chasma Boreale and a now-buried chasma. The lowermost sequence, named "radar unit PLD1" corresponds to units C and D mapped by Putzig et al. (2009).

The aim of this study is to use radar stratigraphy from SHARAD to reconstruct the first stages of water ice accumulation and climatic changes of the Martian NPLD. Rather than mapping unconformities separating sequences or packets of reflectors (Holt et al., 2010; Putzig et al., 2009) we delineate the stratigraphy of the first ~500 m thick sequence of the NPLD (PLD1 in Holt et al., 2010) in three dimensions at the scale of single radar reflectors. This allows us to determine net accumulation and retreat phases via strata geometries and qualitatively compare those to available NPLD accumulation models based on orbital forcing (Greve et al., 2010; Levrard et al., 2007).

2. Methods

2.1. Dataset, interpretational approach and data processing

This study is based on reflector tracking within radargrams acquired by SHARAD. SHARAD is an orbiting nadir-looking chirped radar sounder with a central frequency of 20 MHz and a 10 MHz bandwidth, allowing a theoretical vertical resolution of ~8.4 m in water ice after pulse compression (Seu et al., 2007, 2004). The radiation pattern of the dipole antenna, combined with range and Doppler focusing, result in a horizontal ground resolution of 0.3–1 km along-track and 3–6 km across-track (Seu et al., 2007). The SHARAD dataset used in this study consists of approximately 2700 profiles crossing the NPLD. In these profiles, the vertical axis represents two-way time delay of surface and subsurface radar echoes detected by the instrument, and the horizontal axis represents the distance along ground track travelled by the spacecraft.

SHARAD is capable of penetrating the NPLD through its full thickness of up to 2.3 km, and its ability to detect internal stratigraphy is limited only by the spacecraft orbital geometry and the presence of steep scarps at the surface. The former results in a circular area north of 87.2° where no radar profiles are available, while the latter cause distortions of subsurface reflectors or prevent their reception, creating "shadow zones." Reflector correlation directly through these areas is usually not possible, but the extensive and dense data coverage allows the interpreter to follow reflectors around steep scarps using orbital track intersections in many cases.

In this study, reflectors are assumed to represent isochronous surfaces and to result from changes in the concentrations of dust that significantly alter the dielectric constant (Nunes and Phillips, 2006; Phillips et al., 2008).

A set of 9 horizons, each corresponding to a unique reflector, was tracked across 700+ radargrams in a seismic data interpretation environment (Halliburton's Landmark DecisionSpace) (Fig. 2). Horizons are labeled with single digit numbers according to their relative position in the stratigraphic column, starting from 1 near the base to 7 near the top of the sequence. The only exception to our reflector tracking procedure is horizon 4, which corresponds to the top of a set of two closely spaced reflectors whose separation often falls close or below SHARAD's vertical resolution. The lateral extent of each horizon is guaranteed by tracking only continuous and coherent amplitude peaks, which are semi-automatically detected and tracked by the interpretation software. This latter function helps the interpreter to delineate the peak signal of a reflector with consistency, therefore reducing the subjectivity of horizon tracking. Two stacked horizons define an accumulation unit, designated herein by the top horizon's label (e.g. the packet of material between horizons 2 and 3 is called "unit 3").

The resulting delay-time interpreted dataset is depth-converted assuming a bulk NPLD composition of water ice with minor impurities ($\varepsilon_r = 3.1$, Grima et al., 2009), and then referenced to the surface MOLA topography. In some cases, imperfections in the original delay-time profiles and MOLA topography cause the depth-conversion process to introduce artifacts that appear as a small set of points (typically less that 3–4) with drastically different elevations with respect to adjacent data. These are treated as outliers and removed from the dataset during a quality check analysis before any further analysis is performed.

Depth corrected data are then imported in ESRI ArcMap for analysis and gridding. The point datasets are gridded with the natural neighbor interpolation. Albeit a non-exact interpolation technique, the difference between the original points and the final surface does not exceed a few meters on average, well below the 8.4 m resolution of SHARAD in NPLD materials (Seu et al., 2007). The resulting 3D surfaces represent NPLD paleosurfaces or, in other words, snapshots of subsequent stages of the initial NPLD growth. Thickness maps are computed by subtracting the elevation of raw data points along a paleosurface from the overlying ones, thus showing accumulation and/or erosional patterns of each unit. Raw data points are used in this calculation to avoid the introduction of error due to interpolation of single paleosurfaces.

2.2. Unit thickness error analysis

The unit thickness computed in this study is affected by errors that arise from (1) the finite SHARAD vertical resolution and (2) subjectivity in reflector tracking. The first error source is often assumed to be equivalent to the theoretical vertical resolution of SHARAD in water ice as determined by its chirp bandwidth (8.4 m; Seu et al., 2007). However, processing of the radar data involves the application of a Hann window that reduces the amplitude of sidelobes at the expense of broadening the echo main lobes to about twice their original half-power width (Nunes and Phillips, 2006). This does not change the vertical location of reflectors in profiles, since the peak amplitude is at the same time delay; therefore, isolated interfaces may still be identified at the SHARAD theoretical resolution of 8.4 m (Christian et al., 2013; Seu et al., 2007). However, two closely spaced interfaces may result in adjacent reflection peaks that interact with each other, resulting in an even broader signal and reducing the interface resolving capabilities to 10–20 m, depending on the relative strength of the two reflectors (Nunes and Phillips, 2006). In our study, all but one of the tracked reflectors (horizon 4, as noted previously) have a single narrow peak and have spacing from other reflectors multiple times larger than the conservative 20 m proposed by Nunes and Phillips (2006), therefore the theoretical SHARAD resolution of 8.4 m (Seu et al., 2007) is assumed to represent the data uncertainty, unless otherwise noted.

As briefly illustrated in the previous section, reflector tracking in a radar profile is performed with the aid of a software algorithm that automatically identifies the peak amplitude within a delay-time window defined by the interpreter. This software functionality reduces the magnitude of the subjectivity error component, but is not guaranteed to completely eliminate it. To estimate the magnitude of the remaining subjectivity error, an independent interpreter with training in radar profile analysis but no prior knowledge of the study site stratigraphy was asked to track reflectors along a sample profile (Fig. S1a). The resulting depth-converted data were then compared to the main interpreter's measurements, showing an average absolute difference of 0.64 m (Fig. S1b).

Once the magnitudes of contributing error sources are known, the absolute error in thickness is calculated as

$$E_{thick} = \sqrt{E_{rad,u}^2 + E_{rad,l}^2 + 2E_{subj}^2}$$

where E_{thick} is the absolute error in unit thickness, $E_{rad,u}$ and $E_{rad,l}$ are the uncertainties of SHARAD data in NPLD materials in the upper (u) and lower (l) reflectors, respectively, and E_{subj} is the estimated subjectivity error. Using $E_{rad,u} = E_{rad,l} = 8.4$ m (theoretical SHARAD vertical resolution in water ice; Seu et al., 2007), and $E_{subj} = 0.64$ m, the absolute thickness error is $E_{thick} = 11.9$ m. This figure is assumed to be valid for all units, except where the reflector doublet of horizon 4 delineates the upper or lower boundary of a unit (i.e. units 4 and 5 in some locations). In this case, the conservative 20 m resolution proposed by Nunes and Phillips (2006) is used for $E_{rad,u}$ or $E_{rad,l}$, obtaining an $E_{thick} = 21.7$ m.

2.3. Terminology

In this study, the following terminology is used in the analysis and interpretation of radar profiles and derived products.

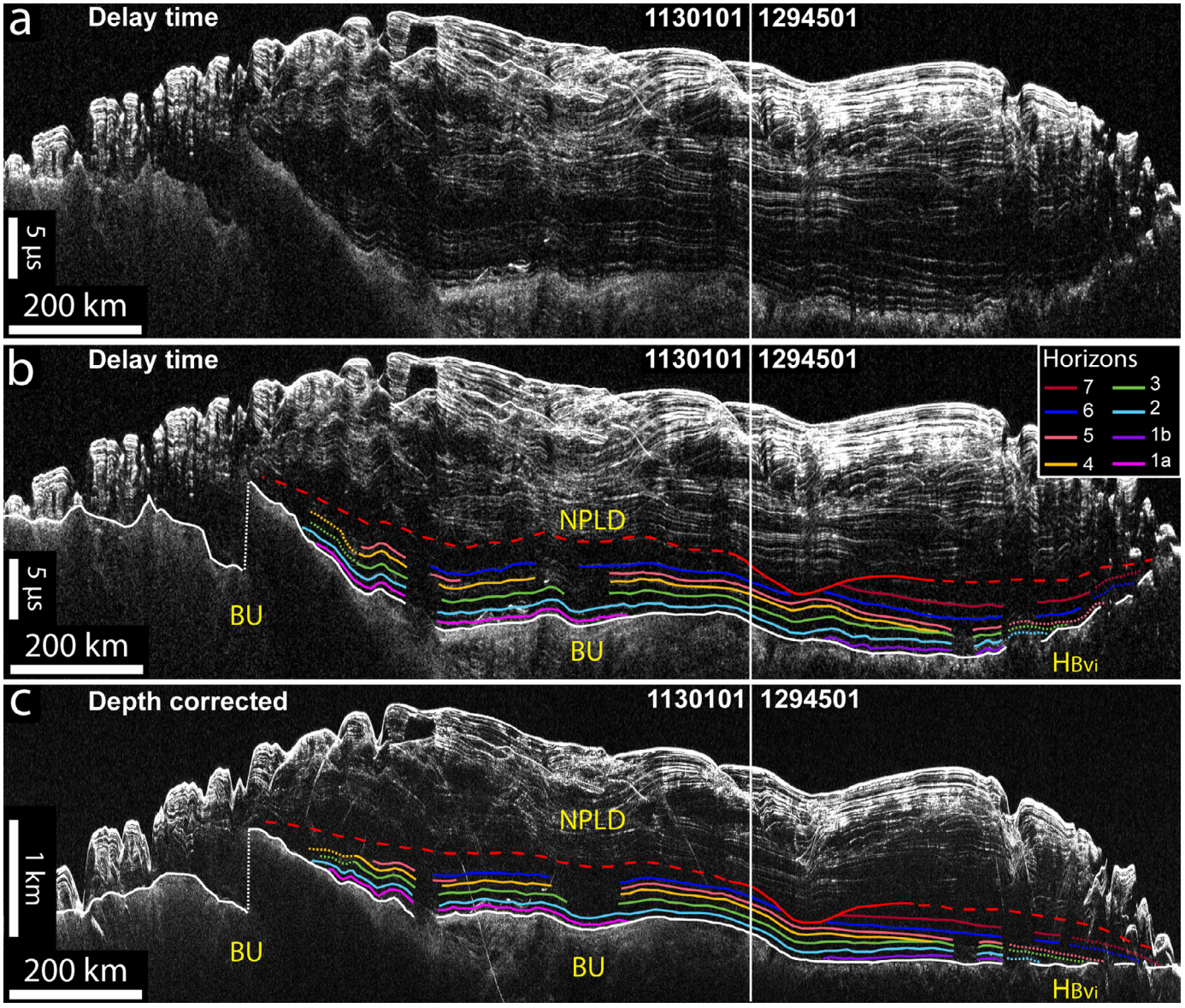

Fig. 2. SHARAD internal stratigraphy across Planum Boreum. (a) Two-Way-Time (TWT) combined radargram spanning two intersecting orbital tracks (location in Fig. 1). (b) Stratigraphic interpretation of the lowermost NPLD for this transect. (c) Depth corrected radargram assuming a bulk NPLD composition of water ice ($\varepsilon_r = 3.1$, Grima et al., 2009). The red line on top corresponds to a major angular unconformity (solid line) and its correlative conformity (dashed line) that bounds the top of the lowermost NPLD mapped by Holt et al. (2010). Dotted lines indicate horizon locations which were difficult to map due to weak reflectors. Note the pinch-outs of the two lowermost horizons (1a and 1b, pink and purple respectively), which onlap the BU and HBv_i unit. (For interpretation of the references to color in this figure legend, the reader is referred to the web version of this article.)

- *Pinch-out*: A wedge-shaped termination of a layer that gradually thins or tapers out until reaching zero thickness.
- *Reentrant*: A morphologic feature formed by low elevation terrain enclosed on all but one side by higher topography.

3. Results

3.1. Overall view

Detailed mapping of radar reflectors throughout the lowermost NPLD delineates a total of eight units (Fig. 2). Five units exhibit only minor thickness variations across the mapped extent of Planum Boreum, in agreement with previous studies that revealed the thickness uniformity of NPLD layers, packets and sequences (Holt et al., 2010; Phillips et al., 2008; Putzig et al., 2009). Conversely, three units exhibit significant thickness variations (Fig. 3) and reduced lateral extent compared to the other units (Fig. 4a,b).

The geometry of paleosurfaces generally mimics the basal topography of the NPLD (Fig. 2), with the exception of slightly thicker, upper deposits within reentrants in the BU (Fig. 4b,c). Most units are also slightly thicker at higher elevations, but become gradually thinner when approaching the BU high in the sector 250-290° E. All units tend to pinch-out when approaching the outer boundaries of the NPLD, although in places this observation is based on inference from overlying radar stratigraphy due to loss of reflectors beneath dense troughs and steep scarps near the margins.

Each radar unit is characterized by consistent thinning along the BU slope beneath the so-called “saddle region” between the main lobe and Gemina Lingula (Fig. 3). Moving south from the

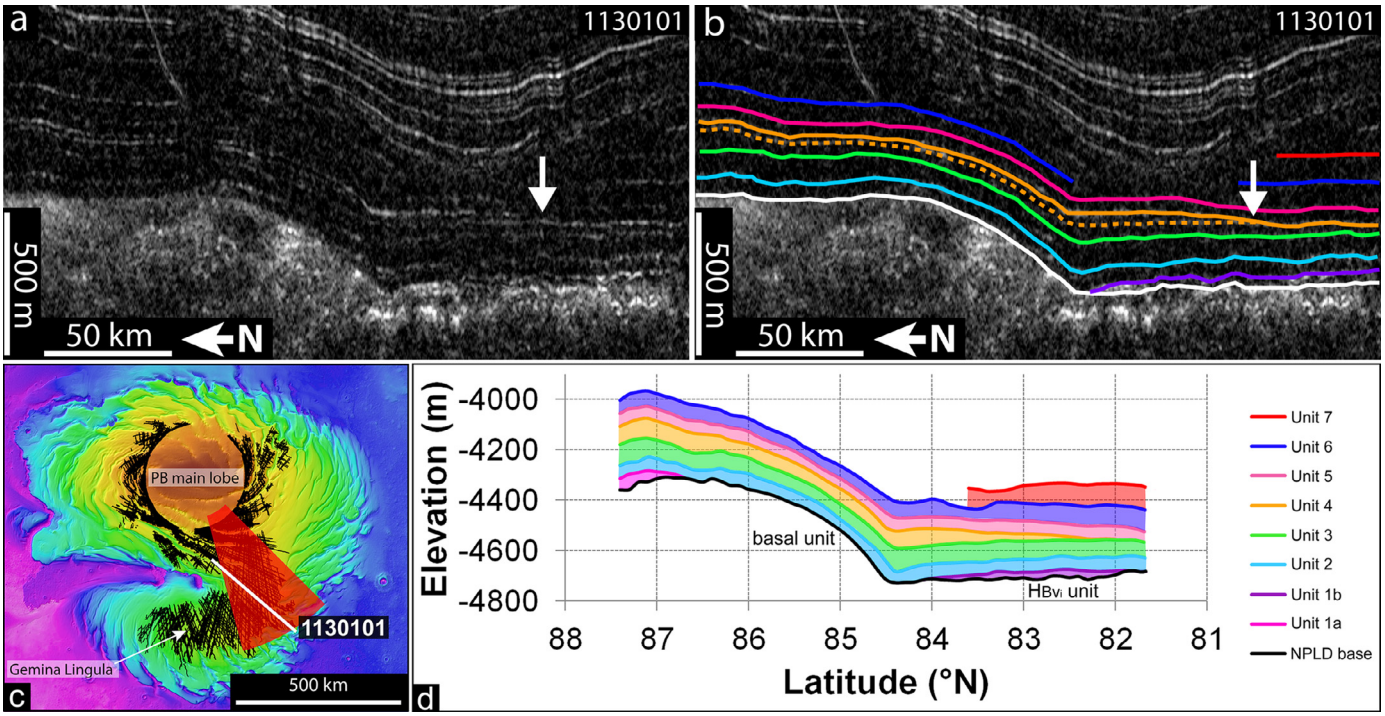

Fig. 3. (a) Original and (b) interpreted sample of depth-corrected radargram 1130101 (location in panel c) showing details of the lowermost NPLD stratigraphy along the BU slope in the "saddle region" between Gemina Lingula and the PB main lobe. Note the pinch-outs of units 1b (purple) and 4 (orange) and the thinning of all units along the BU slope. Also note the presence of a reflector (orange dotted line) and pinch-out (white arrow) in the upper portion of unit 4. (c) MOLA elevation map of PB showing the mapped extent of horizons 1 through 7 (black lines) and location of data shown in other panels. (d) Averaged horizon elevations in the sector 15°-45°E 81.5°-87.2° N (red shade in the map in panel c). Note the pinch-outs of units 1a, 1b and 4, and the thinning along the BU slope at latitudes 84.5-86° N. (For interpretation of the references to color in this figure legend, the reader is referred to the web version of this article.)

slope break, unit thicknesses increase and then decrease again until the units terminate.

Each horizon, with the only exception of 1a, is truncated by a major erosional unconformity that bounds the top of the sequence, mapped by Holt et al. (2010) (Fig. S2). This unconformity delineates a buried chasma that extends within the eastern part of the NPLD (Holt et al., 2010). The same concave up chasma morphology appears from the spatial distribution of the erosional truncation of horizons in that region.

The units described below exhibit characteristics that are significantly different than large-scale, homogenous accumulation.

3.2. The oldest NPLD: units 1a and 1b

The lowermost accumulation in the NPLD is characterized by two similar, but disconnected, units that are located immediately above the BU (unit 1a) and Vastitas Borealis interior unit (unit 1b) (Fig. 4a).

Unit 1a lies within Planum Boreum's main lobe and is characterized by a very broad, quasi circular dome shape with an average thickness of ~41 m. Its center is slightly shifted from the North Pole toward Gemina Lingula, while the thickest portion is located on the western side, at the base of a BU topographic high. A sudden pinch-out, observed consistently in hundreds of radargrams (Example in Fig. 2), delineates the southern edge of this unit (Fig. 4a, marked by a blue line). Thinning also occurs at the head of a BU reentrant mapped by Brothers et al. (2015) (Fig. 4a).

Unit 1b is located in the Gemina Lingula region and terminates laterally with pinch-outs toward both the North Pole and the equator (Example in Fig. 2). It appears to mantle and attenuate the roughness of the Vastitas Borealis interior unit, thus the thickness is largely uniform with minimal local variations (average ~36 m). Unit 1b represents the lowermost deposit in Gemina Lingula and its shape (Fig. 4a) is reminiscent of the unconformity bounded proto-Gemina Lingula delineated by Holt et al. (2010) (Fig. 2).

3.3. Evidence of retreat in unit 4

Unit 4 also exhibits an equatorward pinch-out located within Gemina Lingula (Example in Fig. 2). This termination approximately follows the 82nd parallel (Fig. 4b). The thickness map shows subtle reentrants along its border (Fig. 4b, cold colors). Radar mapping of horizon 4 was complicated by the fact that it is composed of two tightly spaced reflectors that merge in multiple locations (as discussed in Section 2.2 and illustrated by Nunes and Phillips, 2006). Although continuous tracking of each of these reflectors is generally possible, their separation is very close to the estimated thickness error of 21.7 m for this particular configuration, and their mapping would probably result in a mere test of radar resolution. Therefore, we decided to analyze the internal structure of unit 4 in a qualitative way, delineating a second, stratigraphically higher pinch-out (the southward termination of the upper reflector, noted by white arrow in Fig 3a,b) that is shifted ~125 km toward the North Pole with respect to the main unit 4 termination (Fig. 4b, white dotted line).

3.4. Undulating pattern in unit 7

The thickness map of unit 7 shows a distinctive pattern of undulating thickness within Gemina Lingula (Fig. 5). We note that this pattern arises from irregularities in the bounding surfaces of this unit, horizon 6 and 7: they are characterized by very similar stratigraphic geometries, but the uppermost horizon appears to be shifted toward the PB main lobe by at least 10 km (Fig. 5c). This configuration is reminiscent of the cyclic step architecture described by Smith et al. (2013) and has the same structural

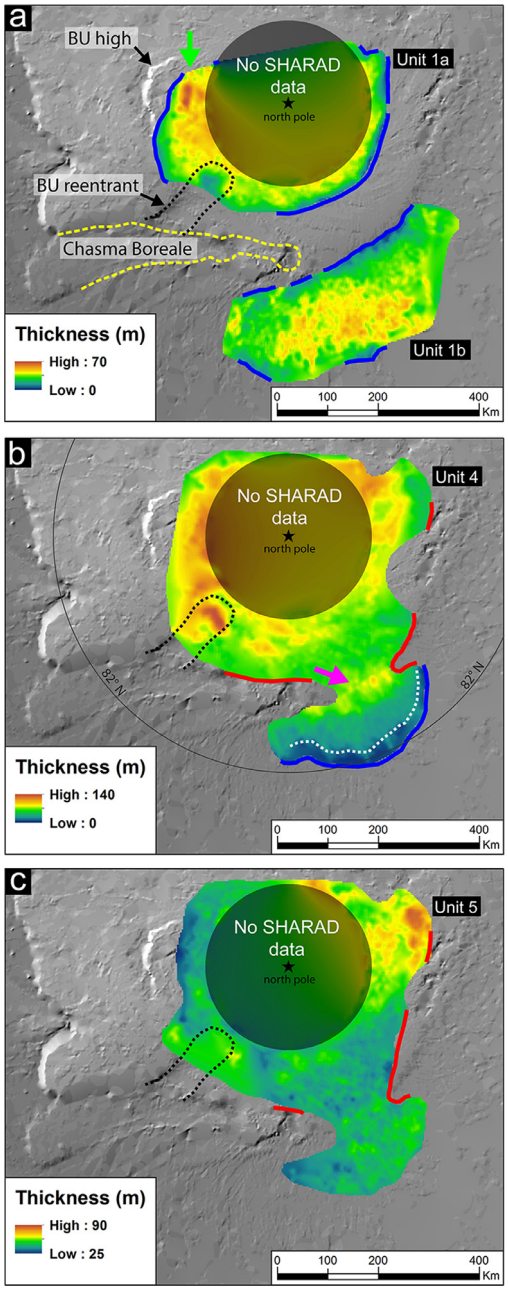

Fig. 4. Thickness maps of four units mapped in this study, superimposed on the shaded relief map of the basal unit resulting from SHARAD mapping (Brothers et al., 2015). Blue lines delineate pinch-out terminations mapped in radargrams, red lines delineate reflector terminations resulting from later erosion that carved the proto-Chasma Boreale in the west and a now-buried chasma in the east (Holt et al., 2010), black dotted lines delineate the lateral boundary of a reentrant in the BU mapped by Brothers et al. (2015), and the yellow dashed line follows the edges of present-day Chasma Boreale. (a) Thicknesses of the two oldest units in the NPLD, unit 1a and 1b. Note the pinch-outs appearing in cold colors. A net accumulation gap is present between the two deposits. Accumulation is also significantly reduced within the BU reentrant. Unit 1a thickness increases at high latitudes and elevation, but rapidly translates into a pinch-out to the west toward the BU high (green arrow). (b) Thickness of unit 4. Note the cold colors indicating a pinch-out on the southern extreme of the unit, and the increase in thickness just south of the BU slope (pink arrow, warm colors). The white dotted line delineates the location of the pinch-out of a reflector within the upper portion of Unit 4 (see also Fig. 3a,b, white arrow). Accumulation reaches the absolute maximum for this unit within the BU reentrant. (c) Thickness of unit 5, showing significant shift of net accumulation to the east compared to unit 4; similarly to unit 4, thickness reaches a local maximum near the BU reentrant, indicating persistent high net accumulation in this area. (For interpretation of the references to color in this figure legend, the reader is referred to the web version of this article.).

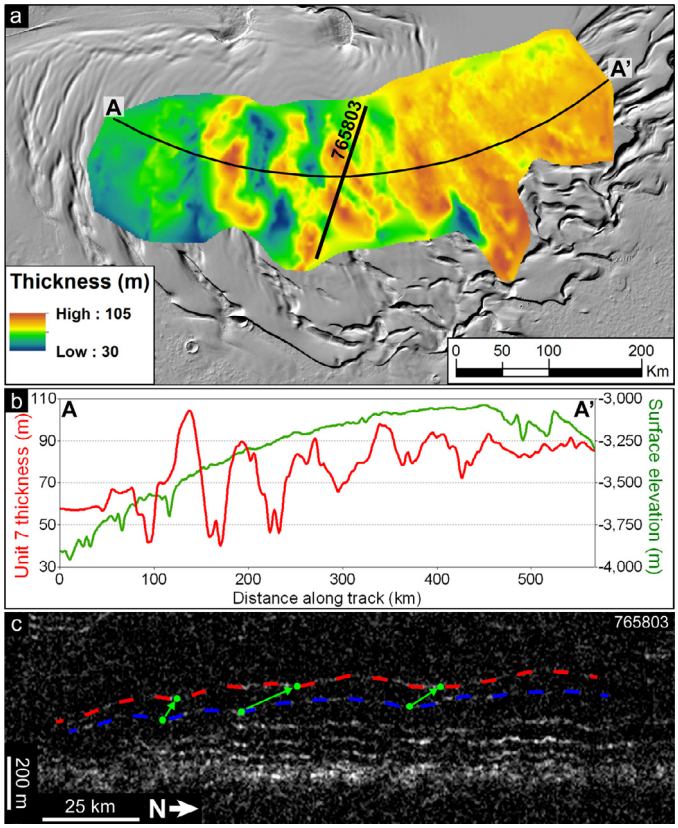

Fig. 5. (a) Thickness map of unit 7, showing a longitudinal undulating pattern. (b) Thickness and elevation profile along the 82nd parallel (A-A′ line in panel a). Note the quasi-periodicity in the varying thickness and absence of correlation with the modern surface elevation of Gemina Lingula. (c) Depth-corrected radar profile showing that variations in unit 7 thickness arise from undulating geometry of horizon 6 and 7 (blue and red dashed lines, respectively). The green dots are located on local elevation minima, and appear to indicate an uphill migration (green arrows). Also note the southward pinch-out terminations of units 1b, 2 and 3 (unmarked reflectors below blue dashed line); unit 4 terminates with a pinch-out on unit 3 just north of this radar profile (see Fig. 4b). (For interpretation of the references to color in this figure legend, the reader is referred to the web version of this article.).

orientation of the modern Gemina Lingula surface. However, the thickness undulations have different wavelengths compared to those of the surface topography, confirming that this is not an observational artifact (Fig. 5b).

4. Discussion

Our study shows that the topography of the earliest NPLD evolved by gradual stacking of ice units, with alternating growth and shrinkage of the net ice accumulation area. Deposits in the lowermost NPLD generally drape the pre-existing topography, with the exception of unit 1a, 1b and 4, which are characterized by limited areal extent compared to the other units. Increased thickness in younger units (especially units 4, 5 and 6) correlates well with depressions and reentrants within underlying units (Fig. 4), suggesting that topography may play an important role in controlling where water ice preferentially accumulates. In addition, units tend to pinch-out approaching the BU high next to the pole, and become thicker in locations of the main lobe farther from the pole and in Gemina Lingula (Fig. 3). These findings challenge the predictions of larger net ice accumulation at high latitudes, where ice stability should be favored due to lower average incident solar radiation during low obliquity cycles (Greve et al., 2010; Laskar et al., 2002; Levrard et al., 2007). Thickness maps also indicate that the major net accumulation centers shifted with time (Fig. 4),

suggesting that additional localized or regional forcing is superimposed on global controls on water ice stability. We will proceed with a discussion on the possible mechanisms that drove these variable and changing patterns of water ice deposition and erosion during the earliest NPLD deposition.

4.1. Topographic controls

Topography alone may have driven the formation of morphological anomalies in the lowermost NPLD by (1) creating cold traps, (2) casting shadows near steep margins, (3) increasing the incidence angle of solar radiation, and/or (4) influencing the direction and strength of katabatic winds.

Some low-lying areas, such as the BU reentrants mapped by Brothers et al. (2015) (Fig. 4a), may have acted as cold traps if stationary masses of cold air could collect there stably. However, all of the reentrants have wide openings that likely allowed winds to move cold air masses out of the depressions, therefore hindering the cold trap mechanism.

Another possible mechanism to enhance accumulation is shadowing near the flanks of the reentrants, which would have prevented sunlight from reaching the floor at low sun elevation angles. We would expect this effect to diminish over time as ice continued to accumulate within the reentrant and the flanks became less pronounced; however, this is incompatible with the observation of increasing thicknesses of units 2 to 5 compared to unit 1a thinning in these regions (Fig. 4).

Conversely, exposure to solar radiation should increase along equator-facing slopes. Model results in Aharonson and Schorghofer (2006) show that equator facing slopes cause mean insolation and surface temperatures to increase with respect to horizontal surfaces at mid latitudes. A similarly comprehensive and quantitative analysis of ice sublimation due to solar radiation dependent on surface orientation at polar latitudes is beyond the scope of this study. Nonetheless, we can speculate that the higher sunlight incidence angle likely contributed to reduced stability of water ice on equator-facing slopes. Moreover, this effect likely became more important as the albedo increased due to the initial accumulation of the bright icy deposits of unit 1a and 1b on flat areas, contrasting with the still dark BU material exposed along slopes. This most certainly had a positive feedback on ice growth, as the surface reflected more radiation toward space and remained cooler. This mechanism—the sudden change of albedo in particular—may have contributed greatly to the development of the accumulation gap between unit 1a and 1b (Fig. 4a). Similarly, subsequent accumulation along the equator-facing BU slope may have been limited due to increased incident solar radiation, resulting in the consistently reduced thickness of units 2 to 6 observed in radar profiles in this region (Fig. 3).

As illustrated by Smith et al. (2013), katabatic winds accelerate down trough slopes, enhancing sublimation of ice, which is later deposited on the opposite lower slope or flat area, where the flow becomes turbulent, thicker and slower after a katabatic jump. In order to develop, katabatic winds necessitate the existence of a significant topographic gradient that would drive the density flow from high elevations down a slope. The roughly domal structure of the basal unit may have been sufficiently developed to initiate katabatic wind flow prior to NPLD accumulation. In this scenario, accumulation of ice is favored at the top of the BU dome, where the katabatic flow is slow compared to the adjacent slope, and in the low-lying areas at the BU slope break (i.e. the proto-Gemina Lingula region). This accumulation pattern can maintain the original BU topographic relief, unless substantial filling of the low-lying areas occurs, causing a reduction of topographic gradient and creating a negative feedback. The stratigraphic architecture of the lowermost NPLD reconstructed in this study reveals that such filling did not occur at this stage. On the contrary, the stratigraphic profile in Fig. 3 shows that about 300 m of ice accumulated in proto-Gemina Lingula beneath unit 7, compared to about 400 m in the main lobe. This difference in thickness is due in part to the limited extent of unit 4, which thins out significantly in the Gemina Lingula region. Thickness maps (Fig. 4b,c) also indicate that some of the high latitude areas of the BU dome, which generally correspond to higher BU elevation, also experienced higher ice accumulation with respect to the low-lying flats of Vastitas Borealis (e.g. the proto-Gemina Lingula region). This must have enhanced the topographic gradient, providing a positive feedback that could have further strengthened katabatic winds.

We therefore argue for a self-sustaining constructional process of the lowermost NPLD in which ice redistribution by katabatic winds maintained—and eventually increased—the original topographic relief of the basal unit, which in turn supported further katabatic flow. Furthermore, a katabatic jump migrates upwind if there is sufficient up-slope erosion and down-slope deposition, as frequently observed in radar profiles across the spiral troughs of the uppermost NPLD by Smith and Holt (2010) and Smith et al. (2013). This type of upslope migration may explain the observed shift of undulating irregularities of horizon 7 with respect to horizon 6 (Fig. 5c), which causes an undulating thickness pattern (Fig. 5a,b). For these reasons, we believe that katabatic winds were the dominant agent that shaped most of the lowermost NPLD, with subordinate effects of increased exposure to sunlight along equator-facing slopes, and possible exceptions for narrow depressions where cold traps may have been the prevailing controls for some periods.

As a qualitative first test of our katabatic wind hypothesis, we analyzed the output of a mesoscale wind model over the BU surface shown in Fig. 8 of Brothers et al. (2015): wind vectors diverge from the northern regions and accelerate down the BU slope, then decelerate in the proto-Gemina Lingula region. These wind velocities and directions suggest that katabatic winds were already present before initial NPLD deposition as predicted in our conceptual model, but further numerical modeling is necessary to fully test our hypothesis.

Laskar et al. (2002, 2004) showed strong variations in Mars' spin axis obliquity and eccentricity over the last 20 My, deeply influencing solar insolation in the north polar area. Likewise, (Phillips et al., 2011) showed that large CO_2 deposits in the SPLD—with a mass equivalent to 80% of present day Mars' atmosphere—may have accumulated during recent times, suggesting that the atmosphere at the inception of NPLD accumulation had different characteristics than today (e.g. higher density and surface pressure). Further wind modeling should test wind regime sensitivity to these variations in orbital and atmospheric parameters.

4.2. Retreat events

A significant feature of the lowermost NPLD is the limited areal extent of three different units (1a, 1b and 4), all laterally bounded by pinch-outs (Fig. 4a,b). The lack of accumulation and the type of termination is due either to (1) one or more erosional events or (2) a reduction of the ice deposition area. In the first case, we would expect to find at least some traces of erosion in the units directly below the pinch-outs, such as angular unconformities, reflector truncations and sudden variations in unit thickness. Instead, all units directly beneath the pinch-outs are laterally continuous and lack any geometric anomaly (Fig. 2). For this reason, we favor the second hypothesis.

Unit 4 is characterized by a major pinch-out in the Gemina Lingula region, followed by a second less prominent pinch-out that is shifted ~125 km toward the North Pole (white arrows in Fig 3a,b,

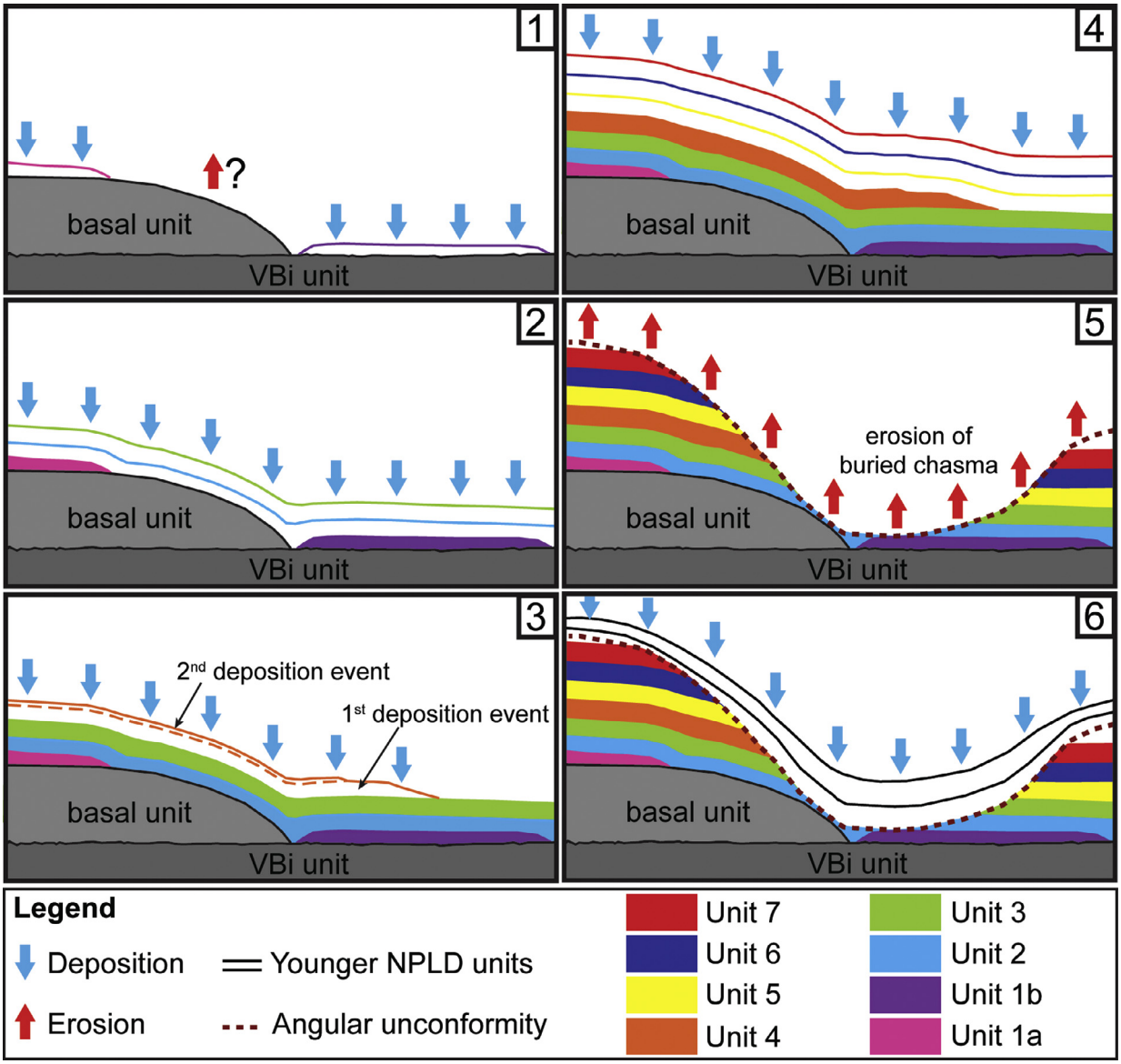

Fig. 6. Step-by-step illustration of the main phases of growth and later partial erosion of the lowermost NPLD.

white dotted line in Fig. 4b). The stratigraphic and spatial location of these two pinch-out terminations describe a progressive, northward reduction of ice extent that is easily explained by two subsequent events of retreat of the ice accumulation area. In a similar way, the anomalously reduced extent of units 1a and 1b compared to the following units, can be explained as the result of a period of limited stability of water ice in Planum Boreum, in particular along the BU slope along which the accumulation gap is located (Fig. 3d, 4a). We propose that katabatic winds and increased solar exposure limited water ice accumulation along the BU slope, resulting into two separate deposits centered around the North Pole and in a small portion of Gemina Lingula. As nearly pure water ice was deposited for the first time in these two areas of Planum Boreum, albedo increased dramatically from the dark BU and VBi unit materials to very bright blankets of ice, further enhancing this depositional contrast. We do not exclude the possibility that erosion could have reshaped these deposits into the observed geometries, but the complete lack of reflector truncations in the accumulation gap areas suggest that erosion was limited in extent or absent.

4.3. Reconstruction of initial NPLD growth

Using the thickness maps and the unit termination trends, we propose a simple constructional step-by-step summary of the lowermost NPLD sequence (illustrated in Fig. 6).

1) Units 1a and 1b were first deposited in limited areas in the PB main lobe and Gemina Lingula regions, possibly followed by erosion that further reshaped them into their current geometries. Notably, the construction of proto-Gemina Lingula as a distinct feature initiates with unit 1b.
2) Widespread water ice accumulation followed, resulting in the creation of units 2 and 3, which extend under most of the present NPLD surface.
3) Unit 4 accumulated in two subsequent stages, recording a simple, progressive retreat of ice deposition toward the North Pole.
4) Other widespread accumulation events followed, resulting in the broad lateral extent of units 5, 6 and 7.
5) Intensive erosion removed ice from units 1b through 7 and reshaped the lowermost NPLD as a whole, forming the

proto-Chasma Boreale and the erosional base of a now-buried chasma.

6) Renewed, widespread accumulation of water ice occurred, including the buried chasma, resulting in a major angular unconformity that bounds upwards the lowermost NPLD sequence (PLD 1 in Holt et al., 2010).

We note that the oldest units in the NPLD, 1a and 1b, accumulated in areas that correspond to two main geomorphic features of PB, the NPLD main lobe and Gemina Lingula. This indicates that the modern shape of the NPLD may be the result of construction, rather than erosion, which began with the onset of ice deposition in PB.

4.4. BU-NPLD contact

The limited extent of the oldest NPLD, immediately overlain by larger, more extensive deposits is indicative of a growing ice sheet that gradually buried the BU (and cavi unit in particular, which extends over large areas underneath the NPLD; Brothers et al., 2015). This scenario agrees well with the cavi-NPLD gradational and laterally transgressive contact observed in visible outcrops in Chasma Boreale (Brothers et al., this issue; Tanaka et al., 2008), and confirms that portions of cavi unit were still exposed and likely undergoing accumulation in some areas during the first phases of NPLD emplacement.

Our reflector mapping also provides fundamental stratigraphic context for the interpretation of the gradational and laterally transgressive contact between cavi unit and the NPLD observed in outcrops. Outcrops displaying the cavi-NPLD transition are relatively scarce and located for the most part along isolated scarps in Chasma Boreale and Olympia Cavi, meaning that only a small fraction of the contact is exposed around Planum Boreum. For these reasons, the reconstruction of the full upper cavi and lowermost NPLD stratigraphy is hard to accomplish in visible outcrops without the integration of a more geographically extensive, observational dataset such as radar profiles. In fact, at least two of the earliest polar layered deposits (units 1a and 1b) are completely buried under younger units, and therefore cannot be mapped in any outcrops. Our radar stratigraphy indicate that these two units predate the lowermost NPLD layers exposed along the gradational and time transgressive contact with cavi (Tanaka et al., 2008), meaning that coeval cavi and NPLD accumulation persisted at least after those two initial water ice deposition episodes.

4.5. Climate information recorded in the lowermost NPLD

The unit extent trends, the thickness anomalies and the stacking pattern of the lowermost NPLD are major, persistent features covering large areas and involving large volumes of water ice, so we interpret them as being fundamentally driven by global climate variations. Laskar et al. (2002) show that insolation on the North Pole of Mars has undergone large cyclic oscillations in the last ~10 Myr, mostly driven by large variations of the spin axis obliquity. The retreat events recorded in the NPLD stratigraphy may be explained with periods of moderately high obliquities, when net ice accumulation is possible only at high latitudes. In a similar way, unit thicknesses may be correlated with the duration of such periods. We find our reconstructed NPLD accumulation history to be qualitatively compatible with the alternating water ice accumulation and retreat phases displayed by models driven by orbital forcing of Greve et al. (2010) and Levrard et al. (2007). Due to the spatial heterogeneity of the units mapped in this study, it is not possible to perform a quantitative comparison of unit thicknesses and net water ice accumulation predicted by the longitudinally averaged models. For the same reason, we conclude that if a correlation between stratigraphy and periodic orbital variations is attempted, one must take into account all lateral variations rather than just a vertical profile of layer thicknesses at one or more outcrops. This work highlights such stratigraphic patterns and shows the presence of depositional and erosional hiatuses that must be taken into account when comparing the stratigraphic record to NPLD accumulation models. Instead of comparing local deposit thicknesses, which we show to vary strongly with locations even at short distances, our work allows average thicknesses and estimated deposit volumes to be compared to the predicted values.

5. Conclusions

Detailed stratigraphic analysis of SHARAD radargrams in the lowermost sequence of the NPLD shows important unit extent and thickness variations that contrast with otherwise uniform layering. In particular, this study found observational evidence of limited geographic extent of some ice units, accumulation gaps and pinch-outs in the two lowermost NPLD units and thinner deposits along equator-facing slopes compared to flat-lying areas at higher and lower latitudes. These observations, together with the analysis of the mesoscale wind model in Brothers et al. (2015), suggest that topographic control over ice net accumulation was significant, hindering ice accumulation over steeper equator-facing slopes due to increased exposure to solar radiation and reworking and transportation by katabatic winds. The spatial heterogeneities observed in unit thickness maps—both horizontally along individual units and vertically through the lowermost NPLD—suggest the presence of multiple water ice depocenters that shifted across the paleo-PB (rather than a single one fixed on the pole), and initiating a proto-Gemina Lingula at the very earliest stages of NPLD accumulation. Two subsequent pinch-outs in the middle part of the sequence suggest a simple northward retreat of ice deposition. The rest of the sequence, instead, is characterized by increased areal extents of overlying units.

The alternating retreat and expansion phases observed in the lowermost NPLD are likely related to climate variations, which, in turn, may be due to orbital forcing. Following a conceptual approach based on orbitally forced NPLD growth models available at this time, we conclude that high spin-axis obliquity induced retreat of the ice sheet and, conversely, low obliquity favored widespread ice accumulation. The earliest stages of NPLD accumulation, as we described here, appear to have captured such swings in obliquity.

The complex stratigraphic patterns and frequent hiatuses present within the lowermost NPLD provide much more specific constraints than were previously available for climate modeling that is driven by orbital forcing, which is both a challenge and an opportunity. Mesoscale modeling using the evolving paleotography that we have mapped could test aspects of our hypotheses regarding the primary processes at work; in particular, the role of katabatic winds.

We have shown that methods traditionally used in stratigraphy analysis on Earth, such as stacking patterns and movement tracking of accumulation centers can be borrowed and adapted to icy deposits on Mars to obtain more complete and simple solutions. This work can be extended within unmapped portions of the NPLD to result in the first detailed reconstruction of NPLD as whole.

Acknowledgments

This research work was supported by NASA Mars Data Analysis Program (MDAP) grants NNX11AL10G and NNX15AM52G. The SHARAD instrument was provided to NASA's Mars Reconnaissance Orbiter mission by the Italian Space Agency (ASI). We thank

Dr. Ajay Limaye and an anonymous reviewer for their constructive comments that substantially strengthened this manuscript.

References

Aharonson, O., Schorghofer, N., 2006. Subsurface ice on Mars with rough topography. J. Geophys. Res. Planets 111, E11007. doi:10.1029/2005JE002636.

Banks, M.E., Byrne, S., Galla, K., McEwen, A.S., Bray, V.J., Dundas, C.M., Fishbaugh, K.E., Herkenhoff, K.E., Murray, B.C., 2010. Crater population and resurfacing of the Martian north polar layered deposits. J. Geophys. Res. Planets 115, E08006. doi:10.1029/2009JE003523.

Becerra, P., Byrne, S., Sori, M.M., Sutton, S., Herkenhoff, K.E., 2016. Stratigraphy of the north polar layered deposits of Mars from high-resolution topography. J. Geophys. Res. Planets 121, 2015JE004992. doi:10.1002/2015JE004992.

Brothers, S.C., Kocurek, G., Holt, J.W., Sequence architecture of the cavi unit, Chasma Boreale, Mars. *Icarus*, (Submitted for publication).

Brothers, T.C., Holt, J.W., Spiga, A., 2015. Planum Boreum basal unit topography, Mars: irregularities and insights from SHARAD. J. Geophys. Res. Planets 120, 2015JE004830. doi:10.1002/2015JE004830.

Byrne, S., Murray, B.C., 2002. North polar stratigraphy and the paleo-erg of Mars. J. Geophys. Res. Planets 107, 11-1-11-12. doi:10.1029/2001JE001615.

Christian, S., Holt, J.W., Byrne, S., Fishbaugh, K.E., 2013. Integrating radar stratigraphy with high resolution visible stratigraphy of the north polar layered deposits, Mars. Icarus 226, 1241–1251. doi:10.1016/j.icarus.2013.07.003.

Cutts, J.A., 1973. Nature and origin of layered deposits of the Martian polar regions. J. Geophys. Res. 78, 4231–4249. doi:10.1029/JB078i020p04231.

Cutts, J.A., Lewis, B.H., 1982. Models of climate cycles recorded in Martian polar layered deposits. Icarus 50, 216–244. doi:10.1016/0019-1035(82)90124-5.

Edgett, K.S., Williams, R.M.E., Malin, M.C., Cantor, B.A., Thomas, P.C., 2003. Mars landscape evolution: influence of stratigraphy on geomorphology in the north polar region. Geomorphology 52, 289–297. doi:10.1016/S0169-555X(02)00262-3.

Fishbaugh, K.E., Byrne, S., Herkenhoff, K.E., Kirk, R.L., Fortezzo, C., Russell, P.S., McEwen, A., 2010. Evaluating the meaning of "layer" in the martian north polar layered deposits and the impact on the climate connection. Icarus 205, 269–282. doi:10.1016/j.icarus.2009.04.011.

Fishbaugh, K.E., Head, J.W., 2005. Origin and characteristics of the Mars north polar basal unit and implications for polar geologic history. Icarus 174, 444–474. doi:10.1016/j.icarus.2004.06.021.

Fishbaugh, K.E., Hvidberg, C.S., 2006. Martian north polar layered deposits stratigraphy: implications for accumulation rates and flow. J. Geophys. Res. Planets 111, E06012. doi:10.1029/2005JE002571.

Galla, K.G., Byrne, S., Murray, B., McEwen, A.HiRISE Team, 2008. Craters and resurfacing of the Martian north polar cap. AGU Fall Meet. Abstr 41, P41B–1360.

Greve, R., Grieger, B., Stenzel, O.J., 2010. MAIC-2, a latitudinal model for the Martian surface temperature, atmospheric water transport and surface glaciation. Planet. Space Sci. 58, 931–940. doi:10.1016/j.pss.2010.03.002.

Grima, C., Kofman, W., Mouginot, J., Phillips, R.J., Hérique, A., Biccari, D., Seu, R., Cutigni, M., 2009. North polar deposits of Mars: extreme purity of the water ice. Geophys. Res. Lett. 36, L03203. doi:10.1029/2008GL036326.

Holt, J.W., Fishbaugh, K.E., Byrne, S., Christian, S., Tanaka, K., Russell, P.S., Herkenhoff, K.E., Safaeinili, A., Putzig, N.E., Phillips, R.J., 2010. The construction of Chasma Boreale on Mars. Nature 465, 446–449. doi:10.1038/nature09050.

Hvidberg, C.S., Fishbaugh, K.E., Winstrup, M., Svensson, A., Byrne, S., Herkenhoff, K.E., 2012. Reading the climate record of the Martian polar layered deposits. Icarus 221, 405–419. doi:10.1016/j.icarus.2012.08.009.

Lalich, D.E., Holt, J.W., 2016. New Martian climate constraints from radar reflectivity within the north polar layered deposits. Geophys. Res. Lett., 2016GL071323 doi:10.1002/2016GL071323.

Landis, M.E., Byrne, S., Daubar, I.J., Herkenhoff, K.E., Dundas, C.M., 2016. A revised surface age for the North Polar layered deposits of Mars. Geophys. Res. Lett. 43, 2016GL068434. doi:10.1002/2016GL068434.

Laskar, J., Levrard, B., Mustard, J.F., 2002. Orbital forcing of the Martian polar layered deposits. Nature 419, 375–377. doi:10.1038/nature01066.

Levrard, B., Forget, F., Montmessin, F., Laskar, J., 2007. Recent formation and evolution of northern Martian polar layered deposits as inferred from a Global Climate Model. J. Geophys. Res. Planets 112, E06012. doi:10.1029/2006JE002772.

Malin, M.C., Edgett, K.S., 2001. Mars global surveyor Mars orbiter camera: interplanetary cruise through primary mission. J. Geophys. Res. Planets 106, 23429–23570. doi:10.1029/2000JE001455.

Milkovich, S.M., Head, J.W., 2005. North polar cap of Mars: polar layered deposit characterization and identification of a fundamental climate signal. J. Geophys. Res. Planets 110, E01005. doi:10.1029/2004JE002349.

Nunes, D.C., Phillips, R.J., 2006. Radar subsurface mapping of the polar layered deposits on Mars. J. Geophys. Res. Planets 111, E06S21. doi:10.1029/2005JE002609.

Phillips, R.J., Davis, B.J., Tanaka, K.L., Byrne, S., Mellon, M.T., Putzig, N.E., Haberle, R.M., Kahre, M.A., Campbell, B.A., Carter, L.M., Smith, I.B., Holt, J.W., Smrekar, S.E., Nunes, D.C., Plaut, J.J., Egan, A.F., Titus, T.N., Seu, R., 2011. Massive CO2 ice deposits sequestered in the south polar layered deposits of Mars. Science 332, 838–841. doi:10.1126/science.1203091.

Phillips, R.J., Zuber, M.T., Smrekar, S.E., Mellon, M.T., Head, J.W., Tanaka, K.L., Putzig, N.E., Milkovich, S.M., Campbell, B.A., Plaut, J.J., Safaeinili, A., Seu, R., Biccari, D., Carter, L.M., Picardi, G., Orosei, R., Mohit, P.S., Heggy, E., Zurek, R.W., Egan, A.F., Giacomoni, E., Russo, F., Cutigni, M., Pettinelli, E., Holt, J.W., Leuschen, C.J., Marinangeli, L., 2008. Mars North Polar deposits: stratigraphy, age, and geodynamical response. Science 320, 1182–1185. doi:10.1126/science.1157546.

Putzig, N.E., Phillips, R.J., Campbell, B.A., Holt, J.W., Plaut, J.J., Carter, L.M., Egan, A.F., Bernardini, F., Safaeinili, A., Seu, R., 2009. Subsurface structure of Planum Boreum from Mars Reconnaissance Orbiter shallow radar soundings. Icarus 204, 443–457. doi:10.1016/j.icarus.2009.07.034.

Seu, R., Biccari, D., Orosei, R., Lorenzoni, L.V., Phillips, R.J., Marinangeli, L., Picardi, G., Masdea, A., Zampolini, E., 2004. SHARAD: The MRO 2005 shallow radar. Planet. Space Sci. 52, 157–166. doi:10.1016/j.pss.2003.08.024.

Seu, R., Phillips, R.J., Biccari, D., Orosei, R., Masdea, A., Picardi, G., Safaeinili, A., Campbell, B.A., Plaut, J.J., Marinangeli, L., Smrekar, S.E., Nunes, D.C., 2007. SHARAD sounding radar on the Mars Reconnaissance Orbiter. J. Geophys. Res. Planets 112, E05S05. doi:10.1029/2006JE002745.

Smith, I.B., Holt, J.W., 2010. Onset and migration of spiral troughs on Mars revealed by orbital radar. Nature 465, 450–453. doi:10.1038/nature09049.

Smith, I.B., Holt, J.W., Spiga, A., Howard, A.D., Parker, G., 2013. The spiral troughs of Mars as cyclic steps. J. Geophys. Res. Planets 118, 1835–1857. doi:10.1002/jgre.20142.

Soderblom, L.A., Malin, M.C., Cutts, J.A., Murray, B.C., 1973. Mariner 9 observations of the surface of Mars in the north polar region. J. Geophys. Res. 78, 4197–4210. doi:10.1029/JB078i020p04197.

Tanaka, K.L., Fortezzo, C.M.. Geologic map of the north polar region of Mars [WWW Document] URL (accessed 3.17.17).

Tanaka, K.L., Rodriguez, J.A.P., Skinner Jr., J.A., Bourke, M.C., Fortezzo, C.M., Herkenhoff, K.E., Kolb, E.J., Okubo, C.H., 2008. North polar region of Mars: advances in stratigraphy, structure, and erosional modification. Icarus 196, 318–358. doi:10.1016/j.icarus.2008.01.021.

Thomas, P., Squyres, S., Herkenhoff, K., Howard, A., Murray, B., 1992. Polar deposits of Mars. Mars 767–795.